DOI: 10.1002/chem.200701384

Quantitative Conformational Study of Redox-Active [2]Rotaxanes, Part 2: Switching in Flexible and Rigid Bistable [2]Rotaxanes

Kirill Nikitin,* Elena Lestini, Jacek K. Stolarczyk,* Helge Müller-Bunz, and Donald Fitzmaurice[a]

Abstract: Translational movement of the macrocycle in two structurally similar bistable [2]rotaxanes, which is induced by a four-step electrochemical process in solution, has been investigated by using a methodology developed in the preceding article (*Chem. Eur. J.* **2008**, *14*, 1107–1116). Both [2]rotaxanes contain a crown ether that can be accommodated by either of two interconnected viologen recognition sites. These sites are substantially different in terms of their affinity towards the crown ether and they possess considerably different electrochemical reduction potentials. The two [2]rotaxanes differ in the length and the rigidity of a bridge that links these sites. A combination of molecular mechanics modelling and NOE spectroscopy data provides information about the conformations of both [2]rotaxanes in the parent oxidation state when the crown ether exclusively populates the strong recognition site. To determine the population of the recognition sites at subsequent stages of reduction, a paramagnetic NMR technique and cyclic voltammetry were used. The key finding is that the flexibility of the connecting bridge element between the recognition sites interferes with shuttling of the crown ether in [2]rotaxanes. It can be demonstrated that the more flexible trimethylene bridge is folded, thus limiting the propensity of the crown ether to shuttle. Consequently, the crown ether populates the original site even in the second reduced state of the flexible [2]rotaxane. On the contrary, in the [2]rotaxane in which two viologen sites are connected by a larger and more rigid *p*-terphenylene bridge, the predominant location of the crown ether at the weak recognition site is achieved after just one single electron reduction.

Keywords: conformation analysis · cyclic voltammetry · molecular modeling · rotaxanes · supramolecular chemistry

Introduction

Self-assembled nanoscale architectures emerged over a decade ago and continue to inspire and motivate researchers in many fields.[1] Potential applications of nanoscale architectures are particularly promising in the field of microelectronics.[2] It is envisaged that the self-assembly of such architectures in solution and at surfaces can be effectively carried out from nanoscale molecular and condensed-phase components.[1,3]

Functional supermolecules, macromolecules and closely related interlocked molecules are attractive nanoscale components and have been extensively studied in solution and at surfaces.[4–7] These nanoscale components have been successfully attached to various nanoparticles and nanostructured electrodes.[8] The properties of such systems can be tuned by controlling the size and composition of the nanoparticles or contact surfaces. However, the functionality depends in particular on the ability to control the orientation and relative positions of the components of these nanoscale systems. For axle-based systems, such as switchable [2]rotaxanes, it is therefore important to ensure that the axle remains normal to the contact surface, the recognition sites located on the axle do not interfere with each other and the recognition sites are restricted from approaching the contact surface. Similar arguments can be made for molecular switch tunnel junctions,[2e] in which the rotaxane molecules should remain stretched between the surfaces of the electrodes. These conditions effectively require the axle of the

[a] Dr. K. Nikitin, E. Lestini, Dr. J. K. Stolarczyk, Dr. H. Müller-Bunz, Prof. D. Fitzmaurice
School of Chemistry and Chemical Biology
University College Dublin
Belfield, Dublin 4 (Ireland)
Fax: (+353) 1-716-2127
E-mail: kirill.nikitin@ucd.ie
jacek.stolarczyk@ucd.ie

Supporting information for this article is available on the WWW under http://www.chemeurj.org/ or from the author.

[2]rotaxane to be rigid, in particular, in the bridging section between the recognition sites.

The orientation of the axle and the stability of attachment has been addressed by using tripodal linkers to adsorb the nanoscale components at the surface of semiconductors or metals.[9] To this end, we have investigated tripodal [2]rotaxanes (Figure 1) that were attached to the surface of TiO_2 nanoparticles and nanostructured electrodes by a tridentate phosphonic acid linker **L**.[10–12] It was possible to electronically address and switch the above [2]rotaxane at the surface of a TiO_2 nanoparticle or at the surface of a nanostructured titania electrode, but the process was accompanied by large conformational changes to the molecule.[12]

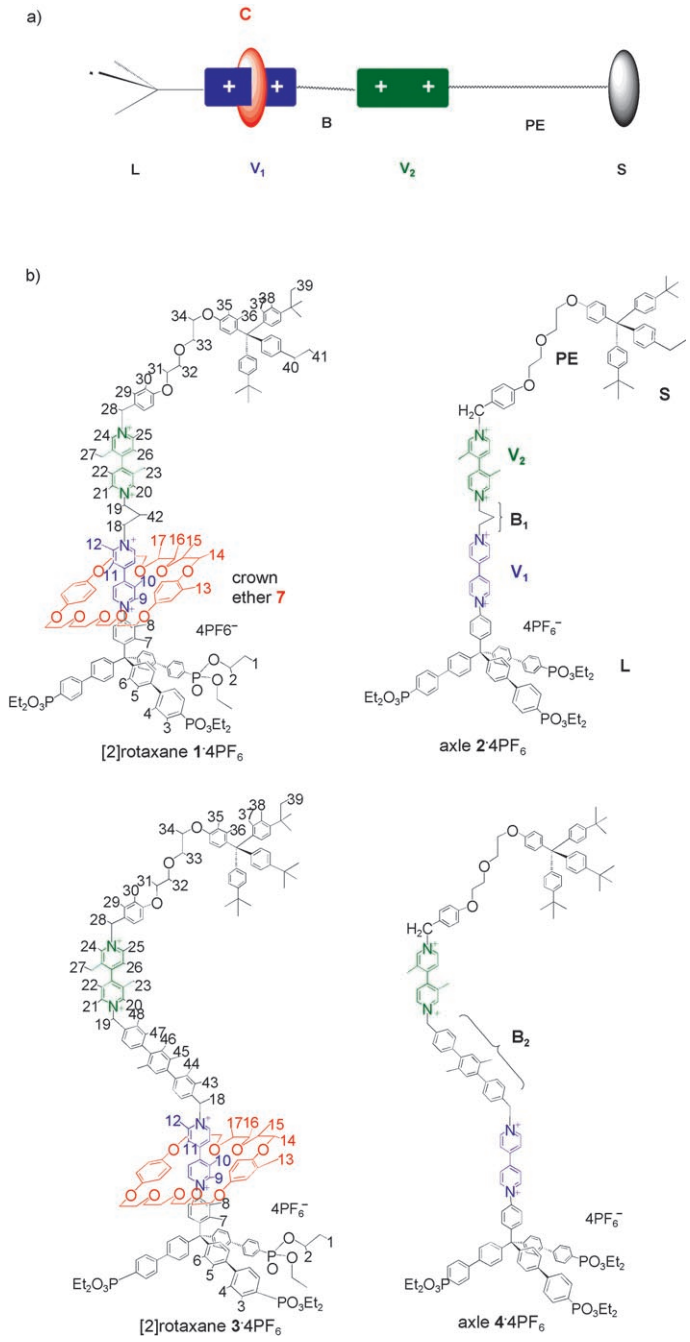

Figure 1. a) General representation of switchable [2]rotaxane in which **L**: linker, **C**: crown ether, $\mathbf{V_1}$ and $\mathbf{V_2}$: viologen sites, $\mathbf{B_1}$ and $\mathbf{B_2}$: bridges, **PE**: flexible chain and **S**: stopper. b) Structures of [2]Rotaxanes **1** and **3**, which show the numbering used in Tables 1, to 4, and axles, **2** and **4**.

In our preceding paper (Part 1)[13a] we presented a novel methodology to quantitatively study the conformations and co-conformations[13b] of [2]rotaxanes in solution and in different oxidation states. We combined molecular modelling with NOESY, paramagnetic line-broadening and suppression spectroscopy (PASSY),[13c] electrochemical and reference crystallographic data to analyse a model, single-station [2]rotaxane. In this paper we apply the same methodology to study two closely related switchable tripodal [2]rotaxanes (**1** and **3**, Figure 1) in solution. The study is directed towards the detailed characterisation of the switching process and its dependence on the overall conformation of the [2]rotaxanes.

A general representation of a switchable tripodal [2]rotaxane is given in Figure 1a. Two different viologen recognition sites ($\mathbf{V_1}$ and $\mathbf{V_2}$) are interconnected by a bridge (**B**) and thread macrocyclic crown ether **C**. The integrity of the system is maintained by the bulkiness of tripodal linker **L** and stopper group **S**, which is connected to $\mathbf{V_2}$ by a flexible polyether moiety **PE**. Although **C** is free, in principle, to travel (shuttle) along the axle, it is predominantly localised at $\mathbf{V_1}$ or $\mathbf{V_2}$.

It has previously been shown that the affinity of **C** to $\mathbf{V_1}$ and $\mathbf{V_2}$ can be altered electro- or photochemically by reducing $\mathbf{V_1}$ and $\mathbf{V_2}$.[14,15] A single- or double-electron reduction leads to a redistribution of **C** between the viologen sites. Studies of shuttling in the above and related [2]rotaxane systems, however, appear to suggest that electrochemical shuttling in [2]rotaxanes may be accompanied by intramolecular stacking of $\mathbf{V_1}$ and $\mathbf{V_2}$ and folding of **B**.[14,15]

The two [2]rotaxanes studied herein differ in the structure of **B** that links $\mathbf{V_1}$ and $\mathbf{V_2}$. In the [2]rotaxane **1**·4PF_6[12] (Figure 1, bridge $\mathbf{B_1}$), the viologens are interconnected by three methylene groups. It is referred to throughout the paper as a flexible rotaxane because the distance between the nitrogen atoms of $\mathbf{V_1}$ and $\mathbf{V_2}$ is relatively short (2.7–5.3 Å) and can, in principle, freely change owing to free rotation. In fact the angle formed by the N···N′ axes of $\mathbf{V_1}$ and $\mathbf{V_2}$ is variable in the range of at least 0 to 180°, thus leaving the possibility for $\mathbf{V_1}$ and $\mathbf{V_2}$ to stack in space. It should also be noted that **1**·4PF_6 contains two flexible units, $\mathbf{B_1}$ and **PE**. To distinguish between the independent movements of these units, the conformational changes are referred to as B-folding and PE-folding, respectively.

The other [2]rotaxane (**3**·4PF_6) incorporates a terphenylene bridge ($\mathbf{B_2}$) between the two viologen stations (Figure 1, bridge $\mathbf{B_2}$). In **3**·4PF_6 the distance between the nitrogen atoms of $\mathbf{V_1}$ and $\mathbf{V_2}$ is relatively long (15.2–16 Å, see the Supporting Information) and does not change significantly as a result of free rotation. For the same reason, the angle formed by the N···N′ axes of $\mathbf{V_1}$ and $\mathbf{V_2}$ is variable in the range of only 0 to 142°, thus excluding the possibility for $\mathbf{V_1}$ and $\mathbf{V_2}$ to stack. Bridge $\mathbf{B_2}$ also effectively plays the role of a spacer between viologens $\mathbf{V_1}$ and $\mathbf{V_2}$.

The aim of this study is to understand the significance of possible intramolecular folding processes and their role in electrochemically controlling the shuttling of **C**. Our findings highlight both the similarities and the differences in behaviour of the flexible and rigid [2]rotaxanes in solution. In particular, they address the question as to whether inserting a rigid bridge into the bistable [2]rotaxane enables more precise control over the position and orientation of self-assembled nanoscale systems. The significance of these findings should be considered in the context of the related studies of molecular shuttles in solution and at the surface.[12–16] Upon completion of the present study it came to our attention that an important and very recent paper is devoted to shuttling in functionally rigid [2]rotaxanes.[16a] It was demonstrated that the rigid spacer possesses a very low barrier for the movement of a macrocycle component in a [2]rotaxane.

This paper describes the design of **1**·4PF_6 and **3**·4PF_6 and the elucidation of their conformations in solution in the parent tetracationic state, $\mathbf{1}^{4+}$ and $\mathbf{3}^{4+}$, from NOE spectroscopy data. The conformations of the radical cations ($\mathbf{1}^{3+\bullet}$ and $\mathbf{3}^{3+\bullet}$) derived from the [2]rotaxanes after single-electron reduction in solution are also discussed. Cyclic voltammetry data are used to elucidate possible conformational changes in $\mathbf{1}^{2+}$, $\mathbf{3}^{2+}$ and $\mathbf{1}^{+}$, $\mathbf{3}^{+}$ reduction states of the [2]rotaxanes.

Results and Discussion

Design of tripodal [2]rotaxanes: [2]Rotaxanes **1**·4PF_6 and **3**·4PF_6 and their corresponding axle components, **2**·4PF_6 and **4**·4PF_6, used in this work are shown in Figure 1.

Both **1**·4PF_6 and **3**·4PF_6 contain tripodal linker **L**. Linker **L** is a large rigid aromatic structure that prevents dethreading of **C**. To provide substantial solubility in most common solvents, the phosphonate groups of **L** are in the form of ethyl esters. **L** is directly and rigidly connected to $\mathbf{V_1}$.

Viologens $\mathbf{V_1}$ and $\mathbf{V_2}$, which are present in **1**·4PF_6 and **3**·4PF_6, are both electroactive and are able to accept up to two electrons each when reduced chemically or electrochemically.[11,12,14] With regards to $\mathbf{V_1}$ and $\mathbf{V_2}$, it should be noted that relatively electron-poor $\mathbf{V_1}$ is fully reduced at significantly more positive potentials than relatively electron-rich $\mathbf{V_2}$.[12] This is possibly because the radical cation of $\mathbf{V_1}$ can potentially form a conjugated planar structure that delocalises the additional electron across both pyridine rings. Further delocalisation is possible because $\mathbf{V_1}$ is conjugated with the *p*-phenylene moiety of **L**. In comparison, as a result of electron density donation from the methyl substituents at the 3 and 3′ positions, viologen moiety $\mathbf{V_2}$ is relatively less electron poor. Additionally, the radical cation of $\mathbf{V_2}$ cannot adopt a planar conformation owing to steric repulsion of the two methyl substituents at the 3 and 3′ positions and cannot delocalise the donated electron.[14f] As a consequence, $\mathbf{V_2}$ is reduced at more negative potentials than $\mathbf{V_1}$ (see below). Owing to the same electronic and steric factors, the affinity of crown ether **7** towards the $\mathbf{V_1}$ and $\mathbf{V_2}$ sites is significantly different. Specifically, affinity of the crown ether to more electron-deficient $\mathbf{V_1}$ is higher than to less electron-deficient $\mathbf{V_2}$. In fact, it has been shown for a closely related interlocked system that the crown ether is located on $\mathbf{V_1}$.[14a,b]

Polyether chain **PE** links $\mathbf{V_2}$ to rigid aromatic stopper **S** in **1**·4PF_6 and **3**·4PF_6. Linker **PE**, which includes adjacent aromatic groups, is 18 Å long in its stretched conformation and is flexible. In Part 1 we demonstrated that owing to its flexibility the **PE** chain adopts a folded conformation and ensures that **7** is localised at the viologen site.[13a] It has been suggested that the folded conformation of the **PE** chain is possibly stabilised by CH–π interactions.

In summary, [2]rotaxanes **1**·4PF_6 and **3**·4PF_6 were designed to contain rigid and flexible moieties in the sequence **L**-$\mathbf{V_1}$-**B**-$\mathbf{V_2}$-**PE**-**S**. Whereas both **1**·4PF_6 and **3**·4PF_6 contain an identical flexible **PE** moiety, the flexibility and size of the central bridging element (**B**) that connects the two functional viologens is significantly different. It is expected that the size of **B** and the B-folding significantly influence the conformation and shuttling in the above interlocked molecules.

Synthesis: [2]Rotaxanes **1**·4PF_6 and **3**·4PF_6 were prepared by a threading method that uses high-concentration conditions[10–12] rather than from axles **2**·4PF_6 and **4**·4PF_6, respectively, with slipping of **7**.[17–19] Owing to the large size of the bulky tetraarylmethane stoppers, the slipping approach would not be successful. The synthesis of **1**·4PF_6 has been described elsewhere.[12] Similarly, the preparation of **3**·4PF_6 and **4**·4PF_6 was carried out as shown in Scheme 1 starting from **8**·PF_6. In the final step, key precursor **12**·3PF_6 was treated with the stopper component, **13** or **13a**, in a minimum volume of benzonitrile.[10] In the presence of **7**, [2]rotaxane **3**·4PF_6 was obtained in good yields, whereas in the absence of **7** only **4**·4PF_6 was formed.

To unambiguously assign the reduction potentials of $\mathbf{V_1}$ and $\mathbf{V_2}$ in compounds **1** to **4**, a direct comparison was made by using structurally analogous model compounds **5**·2PF_6 and **6**·2PF_6. Model compound **5**·2PF_6, which contains $\mathbf{V_1}$ in the absence of $\mathbf{V_2}$, was used to assign the reduction potentials of $\mathbf{V_1}$ in compounds **1** to **4**.[11,12] Model compound **6**·2PF_6, which contains only $\mathbf{V_2}$, was used to assign the reduction potentials of $\mathbf{V_2}$. Compound **6**·2PF_6 was prepared by alkylation of 3,3′-dimethyl-4,4′-bipyridine with **13** (see the Experimental Section). Reference compounds **5** and **6** enabled the comparative structural and dynamic characterisation of **1**·4PF_6 and **3**·4PF_6 in solution.

Conformations of [2]rotaxanes in the parent state: One possible way to characterise the conformations of [2]rotaxanes in their parent states is by X-ray crystallography. This technique has been successfully completed for a number of [2]pseudorotaxanes that contain viologens and crown ethers, but not for [2]rotaxanes that contain bulky, oily stopper groups, which impede the formation of an ordered crystalline phase.[19–21] Until recently, little was known about solid-state and solution structures of viologen-based [2]rotaxanes that incorporate **7**, and in particular, the co-conformation of

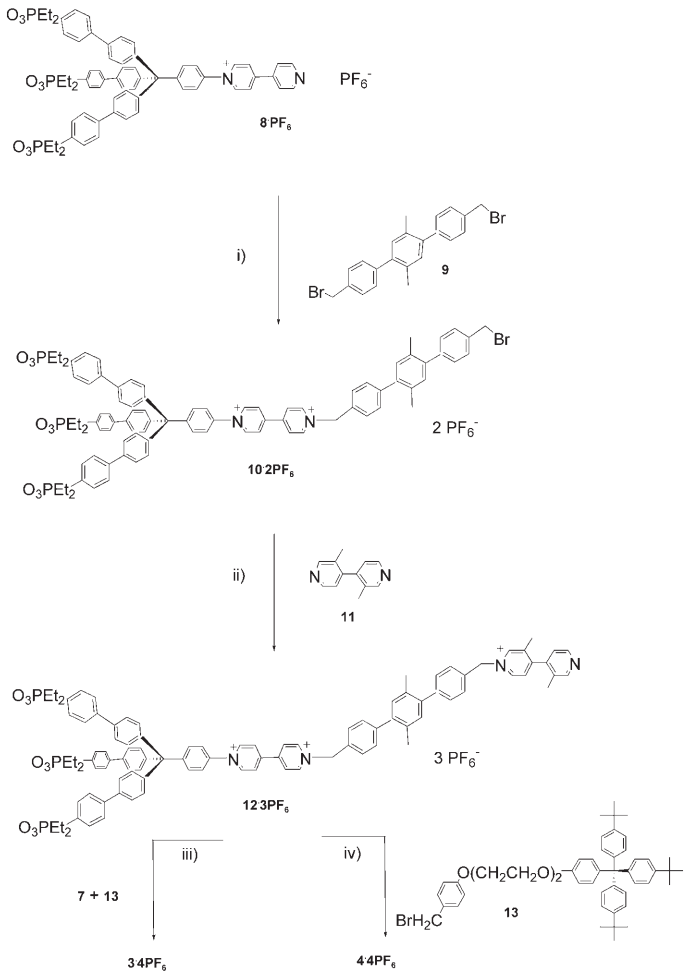

Scheme 1. i) 1) benzonitrile, 36 °C, 2 d, 2) KPF_6 (aq), CH_3NO_2, total 83 %; ii) 1) benzonitrile, ambient temperature, 6 d, 2) KPF_6 (aq), CH_3NO_2, total 83 %; iii) 1) benzonitrile, ambient temperature, 10 d, 2) KPF_6 (aq), CH_3NO_2, total 69 %; iv) 1) benzonitrile, ambient temperature, 10 d, 2) KPF_6 (aq), CH_3NO_2, total 70 %.

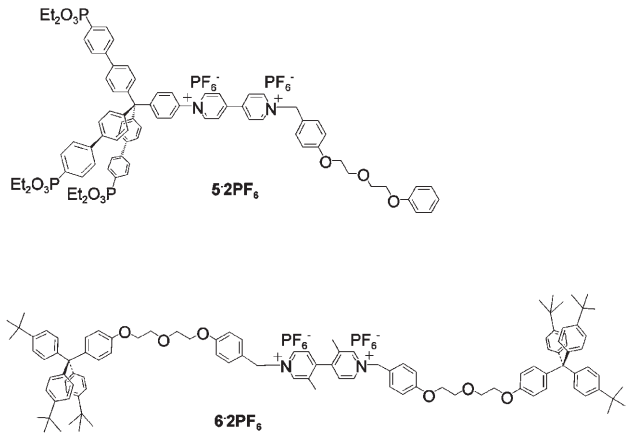

the [2]rotaxanes, that is, which viologen site is predominantly occupied.[12–15]

^{1}H NMR spectroscopy techniques, based on NOE, are commonly used for structural characterisation in solution. In particular, NOE spectroscopy of [2]rotaxanes has been used for this purpose.[22,23] To this end, an almost complete assignment of the observed ^{1}H NMR spectroscopy resonances was carried out on the basis of COSY correlations and related data from structural analogues.[13–15] All of the protons in **1**·4 PF_6 and **3**·2 PF_6 were numbered (Figure 1) so that analogous protons would have the same numbers in the two compounds. For convenience a full list of the chemical shifts, observed NOE intensities and respective calculated distances is given in Table S1 in the Supporting Information. In the aromatic region ($\delta = 7.5$ to 8.0 ppm), some loss of information was unavoidable as a result of overlap of the adjacent peaks.

In Part 1 we demonstrated that a combination of quantitative NOE and crystallographic reference data can form the basis of a detailed analysis of the structure of a model [2]rotaxane in solution.[13a] In this paper we followed the same methodology to characterise two tripodal [2]rotaxanes, **1**·4 PF_6 and **3**·4 PF_6, by using ^{1}H NMR NOE spectroscopy at 298 K in acetonitrile. In separate experiments eight equivalent aromatic protons of **7** (denoted H_{13}) and six methyl protons of the $\mathbf{V_2}$ moiety (H_{23}/H_{27}) were irradiated for both rotaxanes. The results were expressed, as previously, in terms of average effective interatomic distances (d) in **1**·4 PF_6 and **3**·4 PF_6 in solution by using the solid-state crystallographic data from analogous [2]pseudorotaxane and viologen reference compounds.[13a] In this manner two sets of distances were obtained for each rotaxane, distances d_{ax} between aromatic protons H_{13} and other groups of equivalent H_x protons, and distances d_{mx} between methyl protons H_{23}/H_{27} and protons H_x. These results, however, do not allow the conformations and co-conformations of **1**·4 PF_6 and **3**·4 PF_6 to be fully characterised and visualised. Therefore, we used molecular mechanics (MM) minimisation (Macromodel 8.5 with AMBER force field) to find the structures that best matched the experimentally determined distances d_{ax} and d_{mx}. The least-squares method was used for fitting. Owing to the fact that d_{ax} and d_{mx} represent average distances between multiple equivalent irradiated protons H_{13} or H_{23}/H_{27} and multiple protons H_x, it was impossible to directly use them as constraints in MM minimisation. Accordingly, a multiple-step Euler-type optimisation procedure was employed with distance constraints refined during each step to achieve the best fit with d_{ax} and d_{mx}. The resulting optimised structures of **1**·4 PF_6 and **3**·4 PF_6 are shown in Figure 2.

For the calculations of average distances d_{ax} (i.e., when protons H_{13} were irradiated), the corresponding average distance between protons H_{13} and H_{14} in the solid-state structure of an analogous [2]pseudorotaxane was used as a reference (Table 1).[13a] Clearly, crown ether **7** is localised at $\mathbf{V_1}$ adjacent to **L** in both **1**·4 PF_6 and **3**·4 PF_6 in solution. A comparison of **1**·4 PF_6 and **3**·4 PF_6 reveals that in each case there are substantial NOEs for the protons in $\mathbf{V_1}$ (H_9–H_{12} in Figure 1). The calculated distances d_{a9} *to* d_{a12} (from protons H_{13} to protons H_9–H_{12}) are in the range of 3.7 to 4.1 Å, which are similar to the distances in the crystals of analogous [2]pseudorotaxanes.[13a]

It is also clear that **7** is not localised at $\mathbf{V_2}$ adjacent to **S** in both **1**·4 PF_6 and **3**·4 PF_6 in solution. Both **1**·4 PF_6 and **3**·4 PF_6

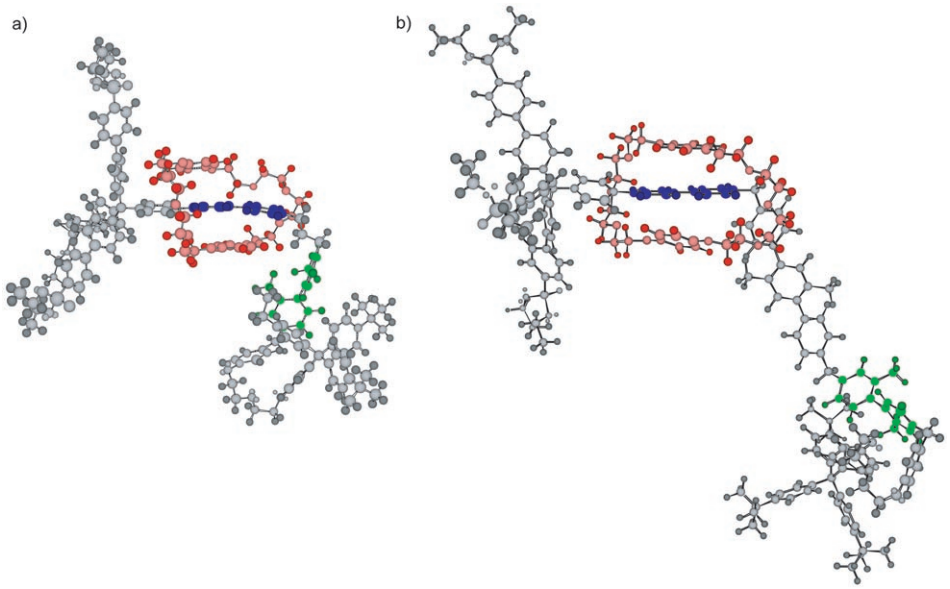

Figure 2. Model conformations of the [2]rotaxanes a) **1**·4 PF_6 b) **3**·4 PF_6.

Table 1. Effective interatomic distances d_{ax} [Å] in **1**·4 PF_6 and **3**·4 PF_6.

Position	Notation	*d* in **1**[a]		*d* in **3**[a]	
		experimental	model	experimental	model
L	H_8	3.73 ± 0.11	4.07	3.96 ± 0.15	4.04
V_1	H_9	4.02 ± 0.16	4.41	4.04 ± 0.16	3.69
	H_{10}	3.82 ± 0.12	4.30	3.71 ± 0.11	3.90
	H_{11}	3.80 ± 0.12	4.37	3.75 ± 0.11	4.19
	H_{12}	4.07 ± 0.17	4.91	4.04 ± 0.16	4.83
7	H_{14}	3.20 ± 0.07[b]	3.39	3.20 ± 0.07[b]	3.28
B_1, B_2	H_{18}	4.40 ± 0.19	5.93	–[c]	5.07
B_1	H_{42}	4.61 ± 0.25	3.83	–	–
B_2	H_{43}	–	–	4.04 ± 0.16	4.22
	H_{44}	–	–	*> 5.86*	4.41
	H_{45}	–	–	5.44 ± 0.06	6.22
B_1, B_2	H_{19}	*> 5.86*	7.13	*> 5.86*	16.12
V_2	H_{23}/H_{27}	6.23 ± 1.04	6.10	*> 6.33*	20.31
	H_{20}/H_{24}	*> 5.86*	7.88	*> 5.86*	18.75
	H_{21}/H_{25}	*> 5.86*	6.94	*> 5.86*	18.41
	H_{22}/H_{26}	*> 5.86*	7.96	*> 5.86*	18.92
S	H_{39}	*> 7.60*	15.03	*> 7.75*	10.59

[a] If no corresponding signal has been observed in the NOE spectrum, the minimum distances (shown in italics) have been estimated on the basis of the noise level in the spectrum and the reference distance d_{ref}. [b] Reference distance d_{ref} was obtained from a crystal structure of a related [2]pseudorotaxane.[13a] [c] The value cannot be accurately determined as a result of overlap with the irradiation peak.

show no measurable NOE of the protons of $\mathbf{V_2}$ (closely overlapping H_{20}, H_{21}, H_{24}, H_{25} and closely overlapping H_{22}, H_{26}). Furthermore, with regards to **B**, which links $\mathbf{V_1}$ to $\mathbf{V_2}$, it is noted that **7** is not localised at the bridge, or in other words, the bridge does not provide a recognition site for **7**. In **1**·4 PF_6, the short distances for bridge methylene protons H_{18} (d_{a18} = 4.40 Å) and H_{42} (d_{a42} = 4.61 Å), but not for the third pair of methylene protons H_{19} (d_{a19} > 5.86 Å) confirm that **7** is localised at $\mathbf{V_1}$. In **3**·4 PF_6, relatively short distances associated with $\mathbf{B_2}$ were calculated for H_{43} (d_{43} = 4.04 Å) and H_{45} (d_{45} = 5.44 Å), however, the distance to H_{19} is far greater than 5.86 Å[24] (16.12 Å in the model of **3**·4 PF_6). The crown ether, therefore, is also not accommodated by $\mathbf{B_2}$. These findings are in full agreement with the expected position of the crown ether moiety in the parent oxidation state.[12,14a,b]

In **1**·4 PF_6, significant NOEs were only measured for the methyl substituents (protons H_{23}/H_{27}), which are, therefore, located relatively close to the crown ether (d_{23} = 6.23 Å), which indicates B-folding of the molecule (Figure 2a). By comparison, it is apparent that the $\mathbf{V_1}$-$\mathbf{B_2}$-$\mathbf{V_2}$ section of **3**·4 PF_6 is not folded because no measurable NOE was detected for the methyl substituents (protons H_{23}) of the $\mathbf{V_2}$ moiety (Figure 2b).

It can be concluded that flexible trimethylene bridge $\mathbf{B_1}$ in **1**·4 PF_6 is folded so that the methyl groups of $\mathbf{V_2}$ can approach **7** from the outside, whereas $\mathbf{V_2}$ as a recognition site does not accommodate **7**. On the contrary, rigid terphenylene bridge $\mathbf{B_2}$ in **3**·4 PF_6 does not permit B-folding and no NOE is detected.

With regards to bulky stopper **S**, no measurable NOE was observed for any of the protons (Table S1 in the Supporting Information). These findings are consistent with the conclusion that **7** populates $\mathbf{V_1}$ and **7** is not approached closer than about 6 to 7 Å by **S**. However, no information can be gained with regards to the conformation and possible folding of the **PE** chain.

Further insights into the structure of **1**·4 PF_6 and **3**·4 PF_6 in solution were obtained when the methyl protons of the $\mathbf{V_2}$ moiety (H_{23} and H_{27}) were irradiated at their respective resonance frequency in subsequent NOE experiments. In this case the required effective reference distance (d^e_{ref}) was calculated between the six protons of the two 3,3′-methyl groups (H_{23}/H_{27} in **1**·4 PF_6 and **3**·4 PF_6) and the two protons at the remaining 3,3′ positions (H_{22}/H_{26} in **1**·4 PF_6 and **3**·4 PF_6). The required structural data were sourced from the X-ray crystal structure of 3,3′-dimethyl-1,1′-diethyl-4,4′-bi-

pyridinium hexafluorophospane, **14**·2 PF_6. The resulting distance (3.79 Å) was used as a reference. The ensuing data are presented in Table 2.

Table 2. Effective interatomic distances d_{mx} [Å] in **1**·4 PF_6 and **3**·4 PF_6.

Position	Notation	d in **1**[a]		d in **3**[a]	
		experimental	model	experimental	model
V_1	H_{12}	*> 8.35*	6.87	*> 8.35*	18.84
V_2	H_{22}/H_{26}	3.79 ± 0.26[b]	3.75	3.79 ± 0.26[b]	3.75
S	H_{39}	6.71 ± 0.84	6.83	7.42 ± 1.15	7.30
	H_{28}	7.27 ± 0.80	6.19	*> 8.35*	5.91
	H_{29}	*> 8.35*	6.36	*> 8.35*	6.09
7	H_{13}	7.38 ± 1.08	6.10	*> 9.44*	20.31

[a] If no corresponding signal has been observed in the NOE spectrum, the minimum distances (shown in italics) have been estimated on the basis of the noise level in the spectrum and reference distance d_{ref}. [b] The reference distance was calculated from the crystal structure of **14**·2 PF_6.

Clearly, in both **1**·4 PF_6 and **3**·4 PF_6 the **PE** chain is folded so that protons H_{39} of the stopper approach the methyl groups of $\mathbf{V_2}$ as close as 6.7 to 7.4 Å. The data also confirm an earlier observation that in the case of **1**·4 PF_6, the methyl groups of $\mathbf{V_2}$ approach **7** at 7.3 Å owing to the B-folding of the trimethylene bridge. No evidence of similar B-folding was found for **3**·4 PF_6 in which the viologens are mechanically separated by non-flexible terphenylene bridge $\mathbf{B_2}$.

The model conformations of **1**·4 PF_6 and **3**·4 PF_6 are presented in Figure 2 in which $\mathbf{V_1}$ and $\mathbf{V_2}$ are highlighted in blue and green, respectively. The crown ether, which forms a sandwich structure with $\mathbf{V_1}$, is shown in red. Whereas the **PE** chain is clearly folded in both **1**·4 PF_6 and **3**·4 PF_6, viologens $\mathbf{V_1}$ and $\mathbf{V_2}$ only form an acute angle in **1**·4 PF_6 as a result of folding of the bridge. In this way, $\mathbf{V_2}$ can come into close proximity with the crown ether. A key finding is that **7** is localised at and interacting with $\mathbf{V_1}$ in both cases.

Conformations of the [2]rotaxanes in the first reduced state: After determining that $\mathbf{V_1}$ was predominantly populated in the parent state and the axles adopted a folded conformation, a further objective of this study was to understand the conformations and co-conformation adopted by **1** and **3** when $\mathbf{V_1}$ was reduced and the affinity of the crown ether towards this recognition site significantly diminished.[25]

Owing to sufficient differences in the reduction potentials between $\mathbf{V_1}$ and $\mathbf{V_2}$ it was possible to selectively reduce $\mathbf{V_1}$ adjacent to **L**. This allowed the co-conformation in the singly reduced radical cation states of **1**·3 PF_6 and **3**·3 PF_6 to be determined by using the paramagnetic relaxation enhancement (PRE) technique outlined below.

Recently we described a novel NMR methodology that allows the structural and conformational changes of the [2]rotaxane molecule in different oxidation states to be monitored.[13a] It was shown that in radical cations of reduced viologens the unpaired electron density causes measurable PRE. The PRE values depend drastically on the distance from the unpaired electron. This provides a means of reasonably accurate characterisation of the location of the macrocycle and estimation of the conformation of the axle in the reduced state of viologen-based [2]rotaxanes.[13a]

The reduction of $\mathbf{V_1}$ can be achieved by using an appropriate reducing reagent or by applying an appropriate negative potential. Typically it is carried out by using Zn metal as a reducing agent. The reduction can be readily achieved for **1**·4 PF_6 and **3**·4 PF_6, the model rotaxanes that only contain the $\mathbf{V_1}$ moiety, and for the model compound **5**·2 PF_6. To determine if this agent also reduces $\mathbf{V_2}$, model compound **6**·2 PF_6, which only contains the $\mathbf{V_2}$ unit, was tested. No evidence for a reduction process with $\mathbf{V_2}$ was found on addition of Zn metal to a solution of **6**·2 PF_6 in either acetonitrile or methanol under air-free conditions. This result clearly indicated that whereas $\mathbf{V_1}$ is reduced, $\mathbf{V_2}$ is not reduced by Zn metal and this reagent can be used to obtain the [2]rotaxanes in singly reduced radical cation states **1**·3 PF_6 and **3**·3 PF_6.

The ^{1}H NMR spectra of **1**·4 PF_6 and **3**·4 PF_6 and their cation radicals **1**·3 $PF_6^{\bullet}$ and **3**·3 $PF_6^{\bullet}$ were recorded in degassed acetonitrile at 25 °C and the relaxation times T_1 were measured by the saturation–inversion method.[13a,c] Calculated PRE values are presented in Tables 3 and 4 (for full T_1 data see the Supporting Information). The effective average

Table 3. Paramagnetic relaxation enhancement and estimated effective distances [Å] in **1**·4 PF_6[a]

Position	Notation	PRE [s^{-1}]	d_x^e
V_1	H_9	PSZ	*< 5.1*[b]
	H_{10}	PSZ	*< 5.1*[b]
	H_{11}	PSZ	*< 5.1*[b]
	H_{12}	PSZ	*< 5.1*[b]
V_2	H_{20}/H_{24}	1.2 ± 0.3	12.0 ± 1.8
	H_{21}/H_{25}	1.0 ± 0.3	12.4 ± 1.9
	H_{23}/H_{27}	7 ± 2	9.0 ± 1.4
B_1	H_{18}	PSZ	*< 5.1*[b]
	H_{42}	PSZ	*< 5.1*[b]
	H_{19}	122 ± 11	5.6 ± 0.6
S	H_{39}	1.3 ± 0.2	11.8 ± 1.5
L	H_5	2.5 ± 0.5	10.6 ± 1.5
7	H_{13}	83 ± 5	5.9 ± 0.7
	H_{14}–H_{17}	58 ± 3	6.3 ± 0.7

[a] -1.00×10^{-2} mol dm^{-3} solution in [D_3]acetonitrile, 25 °C. [b] Based on T_1 below 2.5×10^{-3} s.

Table 4. Paramagnetic relaxation enhancement and estimated effective distances in **3**·4 PF_6.[a]

Position	Notation	PRE [s^{-1}]	d_x^e
V_1	H_9	PSZ	*< 5.1*[b]
	H_{10}	PSZ	*< 5.1*[b]
	H_{11}	PSZ	*< 5.1*[b]
	H_{12}	PSZ	*< 5.1*[b]
V_2	H_{23} H_{27}	0.00 ± 0.09	*> 14*
B_2	H_{18}	PSZ	*< 5.1*[b]
	H_{45}	1.0 ± 0.3	8.1 ± 1.6
	H_{19}	0.0 ± 0.3	*> 14*
S	H_{39}	0.2 ± 0.2	10.6 ± 3.3
L	H_4	0.14 ± 0.07	11.2 ± 2.5
7	H_{13}	26 ± 3	4.7 ± 0.8
	H_{14}–H_{16}	8.4 ± 0.7	5.7 ± 1.0

[a] -10^{-2} mol dm^{-3} solution in [D_3]acetonitrile, 25 °C. [b] Based on T_1 below 2.5×10^{-2} s.

distances from the centre of the paramagnetic suppression zone (PSZ) to each of the proton groups H_x were also calculated.[13a] The distances from the centre of the PSZ to protons H_5 (in the model conformation of **1**·4PF_6) and from protons H_4 (in the model conformation of **3**·4PF_6) were used as references because these distances were expected to remain unchanged upon reduction of the rotaxanes.

The analysis of proton PRE data (Table 3) shows that in **1**·3PF_6, as expected, the strongest paramagnetic effect is experienced by $\mathbf{V_1}$ (protons H_9–H_{12}) and all adjacent protons (PSZ). The PRE is too high to be measured in the PSZ and no quantitative information can be obtained. For the rest of the molecule the proton PRE values were obtained and were used to determine the conformation of the molecule.[13a]

To facilitate the analysis of the co-conformational changes in the [2]rotaxanes upon reduction, the fractions of the ensemble (population) of the rotaxane molecules in which **7** is located at $\mathbf{V_1}$ and $\mathbf{V_2}$ are denoted α_1 and α_2, respectively. Owing to the affinity of the crown ether towards the recognition sites, the sum of α_1 and α_2 should be equal to 1, that is, only the two above co-conformations are considered to be relevant. The values of α_1 and α_2 could also be understood to be the probabilities of finding **7** at either $\mathbf{V_1}$ or $\mathbf{V_2}$, respectively.

Probabilities α_1 and α_2 in the first single-electron reduced state, **1**·3PF_6, were determined as follows: According to Table 3 the PRE value for aromatic protons H_{13} of **7** in **1**·3PF_6 is 83 s^{-1}. If **7** remained at $\mathbf{V_1}$ ($\alpha_1 = 1$) its PRE would be significantly higher, specifically 125 s^{-1} as was previously shown for a structurally similar [2]rotaxane.[13a] However, for **7** located at $\mathbf{V_2}$ the PRE would have been significantly lower, specifically about 7 s^{-1} (Table 3, PRE value for $\mathbf{V_2}$). This may suggest that the population is split between the sites. Assuming that the observed PRE value is a linear combination of the relaxation rates at both sites, it can be calculated that $\alpha_1 = 0.65 \pm 0.10$ in the reduced state **1**·3PF_6, and hence, $\alpha_2 = 0.35 \pm 0.10$.[26] The details of the calculation are given in the Supporting Information. This result suggests that **7** is predominantly, but not completely localised at $\mathbf{V_1}$ in the reduced state, **1**·3PF_6.

The decrease in the PRE value for protons H_{13} can also be interpreted differently. It can be attributed to a shift of the average position of these crown ether protons with respect to $\mathbf{V_1}$, which leads to an increase of the effective distances by a factor of $(^{125}/_{83})^{1/6}$. This corresponds to a shift of only 0.3 Å towards the trimethylene bridge, that is, $^1/_{20}$th of the length of the bipirydyl unit. It means that the crown ether is still structurally localised at $\mathbf{V_1}$. This finding is in qualitative agreement with our previous findings on the surface of titanium oxide.[12]

Note that the PRE values for H_{27} of the methyl substituents in $\mathbf{V_2}$ (7 s^{-1}) are higher than the PRE values for the in-plane aromatic protons H_{20} of $\mathbf{V_2}$ (1 s^{-1}). Consequently, it can be concluded that $\mathbf{V_2}$ in **1**·3$PF_6^{\bullet}$ is folded back towards $\mathbf{V_1}$ so that the methyl substituents of $\mathbf{V_2}$ approach the PSZ of $\mathbf{V_1}$ relatively closely. It can also be concluded on the basis of the noticeable PRE (1.2 s^{-1}) for stopper terminal protons H_{39} that, owing to the folding of $\mathbf{B_1}$ and the **PE** chain, stopper **S** is in the vicinity of the PSZ of $\mathbf{V_1}$. These results prove that B- and PE-folding persist in **1**·3PF_6. This is in excellent agreement with the above NOE findings on the conformation of the parent oxidation state **1**·4PF_6.

To conclude, a single-electron reduction of **1**·4PF_6 in solution does not seem to induce dramatic changes in the population of the recognition sites by **7**. Whereas the interactions of **7** with $\mathbf{V_1}$ are significantly weakened as a result of additional electron density on this site, the crown ether still predominantly populates the $\mathbf{V_1}$ site. This can be explained by considering the folding of the flexible trimethylene bridge, which possibly represents an additional steric barrier for **7** to overcome.

The analysis of the proton PRE data in **3**·4PF_6 (Table 4) shows that in this case, as expected, the strongest PRE is experienced by $\mathbf{V_1}$ itself (H_9–H_{12}) and the surrounding protons (PSZ). Importantly, it is again possible to elucidate the population of the viologen sites by **7** in the first single-electron reduced state **3**·3PF_6. In this case the PRE value for aromatic protons H_{13} of **7** in **3**·3PF_6 is 26 s^{-1}. Following the above argument and by using data from Table 3 for the $\mathbf{V_2}$ site of **1**·3PF_6, it can be calculated that the probability value of α_1 is 0.21 ± 0.10 in the reduced state, **3**·3PF_6, and the probability value of α_2 is 0.79 ± 0.10.[26] The results cannot be explained in terms of shift of the crown ether, as for **3**·3PF_6, because it would require a highly unlikely localisation of the crown at bridge $\mathbf{B_2}$. It can be concluded, therefore, that **7** does predominantly populate $\mathbf{V_2}$ in the reduced state, **3**·3PF_6.

The PRE values for $\mathbf{V_2}$ are negligible. Therefore, as expected, viologen station $\mathbf{V_2}$ in **3**·3PF_6 is not approaching the PSZ of $\mathbf{V_1}$. It can also be concluded on the basis of negligible PRE values for the *t*-butyl groups of the stopper that the stopper does not approach the PSZ of $\mathbf{V_1}$. This is in excellent agreement with the above NOE findings for the parent state of **3**·4PF_6.

Apparently, single-electron reduction of rigid **3**·3PF_6 causes significant changes in the population of the recognition sites by **7** as shown in Figure 3. In this case **7** mainly populates the second, originally weakly binding viologen recognition site $\mathbf{V_2}$.

By comparing the findings for both rigid and flexible tripodal [2]rotaxanes it is concluded, therefore, that as a result of the folded conformation of the axle in **1**, the distribution of the population of the viologen recognition sites by the crown ether is sensitive to, but is not effectively controlled by, single-electron reduction in solution. Upon single-electron reduction the crown ether continues to predominantly populate the originally strongly binding site $\mathbf{V_1}$. On the contrary, the rigid design of **3** provides more efficient conditions for electrochemical control of distribution of the crown ether between recognition sites $\mathbf{V_1}$ and $\mathbf{V_2}$. In this case a single-electron reduction causes inversion of the population, a process that may be termed shuttling or Brownian switching.[27]

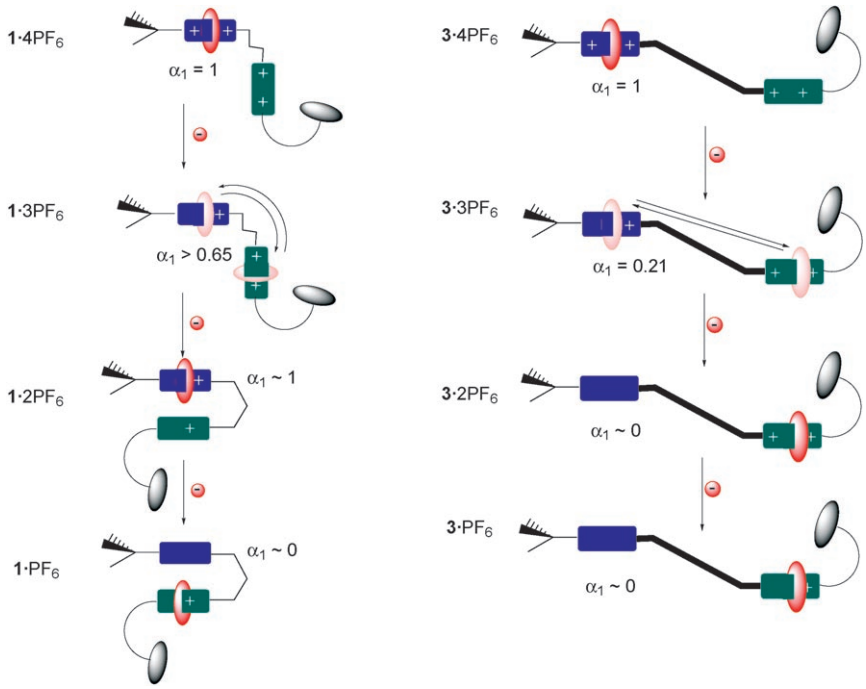

Figure 3. Shuttling in the [2]rotaxanes. Left: flexible **1**·4 PF_6, right: rigid **3**·4 PF_6.

Conformations of the second and further reduced states of 1 and 3: It has previously been shown that cyclic voltammetry (CV) can provide insights into intramolecular shuttling processes in switchable [2]rotaxanes.[11,12,13c,14,15] These insights are possible because the donor–acceptor interaction of **7** with the viologen moieties shifts the reduction potential of the viologens to more negative values. The reduction of viologens is known to be associated with their dimerisation, which leads to positive reduction potential shifts,[28] and with conformational changes, which lead to incomplete reduction.[29] Recently it has been shown that the reduction requires flattening of the structure of the viologens, and consequently, the reduction potentials of viologens depend critically on the dihedral angle between the two pyridinium rings.[14f] Consequently, the reduction requires more negative potentials if the ability of a viologen to adopt a flat conformation is restricted as it is in all 3,3′-dimethylviologens, $\mathbf{V_2}$.

The CVs of [2]rotaxanes **1**·4 PF_6 and **3**·4 PF_6 and the corresponding axles **2**·4 PF_6 and **4**·4 PF_6 were recorded (see the Supporting Information). Tripodal model compound **5**·2 PF_6 and model compound **6**·2 PF_6 were also studied to assign any reduction peaks observed in **2**·4 PF_6 and **4**·4 PF_6. The CV measurements were carried out at a scan rate of 10 $mV\,s^{-1}$ by using a solution of tetraethylammonium hexafluorophosphate (0.05 $mol\,dm^{-3}$) as an electrolyte and non-aqueous $Ag/AgNO_3$ as the reference electrode. The list of the respective peak potentials (E_p) is given in Table 5. For comparison, the reduction potentials of the single-station model [2]rotaxane described in detail Part 1 are also given.[13a]

Owing to the strong overlaps of the reduction peaks of flexible **1**·4 PF_6 and rigid **3**·4 PF_6 in the region at approximately −1 V, it is difficult to make precise assignments of the second and third potentials. For this reason the maxima of combined second and third reduction peaks are quoted for systems **1** to **4**. It is noted that this behaviour was expected on the basis of a number of CV experiments with individual viologen stations $\mathbf{V_1}$ and $\mathbf{V_2}$ and their various mixtures under a range of conditions.

Firstly, let us consider the reduction of bis-viologen system **2**·4 PF_6, which involves four one-electron steps. The assignment of the reduction potentials of **2**·4 PF_6 can be made by comparing the reduction potentials of tripodal model compound **5**·2 PF_6, the $\mathbf{V_1}$ model rotaxane[13a] and model compound **6**·2 PF_6. Owing to the presence of an additional positively charged moiety ($\mathbf{V_2}$) the reduction potential of $\mathbf{V_1}$ in **2**·4 PF_6 is shifted to more positive values compared with tripodal model compound **5**·2 PF_6 (−0.63 V) and model rotaxane (−0.67 V).[14a,b,29] As a result, the first reduction potential of **2**·4 PF_6 is −0.52 V. It can also be concluded qualitatively that the second reduction potential of **2**·4 PF_6 is within −0.96 to −1.0 V, as the second reduction potential of **5**·4 PF_6 (−0.96 V) and the model single-station rotaxane (−1.00 V). The third and the fourth reduction potentials of **2**·4 PF_6 (−1.06 and −1.40 V) are associated with the reduction of $\mathbf{V_2}$. This can be determined on the basis of the reduction potentials of $\mathbf{V_2}$ in **6**·2 PF_6 (−1.07 and −1.55 V).[29] It is concluded, therefore, that the electrochemical reduction of **2**·4 PF_6 involves two single-electron reductions of $\mathbf{V_1}$ followed by two single-electron reductions of $\mathbf{V_2}$. Consequently, the formation of an interim reduced species of **2**·2 PF_6

Table 5. Cyclic voltammetry data.[a]

Compound	E_p [V][b]			
	$\mathbf{V_1}^{2+}\rightarrow\mathbf{V_1}^{+}$	$\mathbf{V_1}^{+}\rightarrow\mathbf{V_1}^{0}$	$\mathbf{V_2}^{2+}\rightarrow\mathbf{V_2}^{+}$	$\mathbf{V_2}^{+}\rightarrow\mathbf{V_2}^{0}$
1·4 PF_6	−0.75	−0.98		−1.46
2·4 PF_6	−0.52	−1.06		−1.40
3·4 PF_6	−0.78	−1.08		−1.58
4·4 PF_6	−0.69	−1.06		−1.48
5·2 PF_6	−0.63	−0.96	–	–
6·PF_6	–	–	−1.07	−1.56
$\mathbf{V_1}$ model rotaxane[c]	−0.77	−1.12		
$\mathbf{V_1}$ model axle[c]	−0.67	−1.00		

[a] Acetonitrile, 25 °C, 0.05 $mol\,dm^{-3}$ tetraethylammonium hexafluorophosphate, 5.00×10^{-2} $mol\,dm^{-3}$ in **1**–**6**. [b] Error bar ±0.01 V. [c] Reference [13a].

with two co-existing viologen radicals, $\mathbf{V_1}^{\bullet}$ and $\mathbf{V_2}^{\bullet}$, is not expected. This species, if formed, would undergo intramolecular viologen–viologen association and lead to pronounced positive shifts in the second and third potentials.

It was possible to analyse the interaction of the same viologen moieties of **1**·4 PF_6 with **7** and the position of **7** after the reduction potentials of the viologen moieties in **2**·4 PF_6 were assigned. The value of the first reduction peak of **1**·4 PF_6 (−0.75 V) is shifted towards more negative values compared with **2**·4 PF_6 (−0.52 V) as a result of the interaction of $\mathbf{V_1}$ with **7**. This is in full agreement with the reduction potentials of the model single-station rotaxane (−0.77 V) and the above NMR spectroscopy findings that the crown ether mainly populates the $\mathbf{V_1}$ site in **1**·4 PF_6, as shown in Figure 3. It also is consistent with previous findings on the surface of titanium dioxide[12] and in solution.[14a,b]

It is expected that in **1**·3 PF_6 the second reduction potential of the $\mathbf{V_1}$ site will be shifted to negative values, possibly to −1.1 V as in the model rotaxane, owing to the interaction with **7** after the first reduction of $\mathbf{V_1}$. This requires, however, the $\mathbf{V_2}$ site to be reduced first at approximately −1.07 V with the formation of two co-existing radical cation viologens (Figure 3). As these viologen radicals are conformationally permitted to interact and dimerise, owing to B-folding, the resulting reduction potential is considerably shifted towards more positive values, −0.98 V. This unexpected shift indicates the early onset of π–π-type stacking of $\mathbf{V_1}$ and $\mathbf{V_2}$ and the crown ether in **1** in comparison with **2**. Finally, the second reduction potential of $\mathbf{V_2}$ in **1**·PF_6 (−1.46 V) is displaced towards more negative values compared with **2** (−1.40 V), which indicates that **7** populates $\mathbf{V_2}$ in the reduced state, **1**·PF_6.[11,12] Proposed co-conformational and conformational changes in **1** in solution are illustrated in Figure 3. It can be concluded that the population of the viologen sites by **7** changes over the course of the four consecutive reduction steps. In first three oxidation states, **1**·4 PF_6, **1**·3 PF_6 and **1**·2 PF_6, crown ether **7** predominantly populates $\mathbf{V_1}$. Predominant population of $\mathbf{V_2}$ takes place in **1**·PF_6 (after triple reduction).

Now let us consider the reduction of the rigid bis-viologen system, **4**·4 PF_6. The relatively long and rigid bridge ($\mathbf{B_2}$) between $\mathbf{V_1}$ and $\mathbf{V_2}$ separates the two stations and prevents B-folding. Accordingly, the reduction potentials of $\mathbf{V_1}$ and $\mathbf{V_2}$ in **4**·4 PF_6 are not shifted to more positive values when compared with $\mathbf{V_1}$ and $\mathbf{V_2}$ in model compounds **5**·2 PF_6 and **6**·2 PF_6, respectively. The first two reduction potentials of **4**·4 PF_6 (−0.69 and −1.06 V) can be assigned, therefore, to $\mathbf{V_1}$. The third and fourth reductions of axle compound **4**·4 PF_6 (−1.06 and −1.48 V) are the reduction potentials of the viologen moiety $\mathbf{V_2}$. The interaction of the viologen moieties in **3**·4 PF_6 with **7** and the position of **7** can be analysed on the basis of the electrochemical shifts. The value for the first reduction of **3**·4 PF_6 (−0.78 V) is displaced, owing to the interaction of $\mathbf{V_1}$ with **7**, towards more negative values compared with **4**·4 PF_6 (−0.69 V). This is in full agreement with above findings by NOE spectroscopy that the crown ether populates the $\mathbf{V_1}$ site in **3**·4 PF_6.

It can be expected that unlike the first reduced state of flexible **1**·3 PF_6, in rigid **3**·3 PF_6 the second reduction potential of $\mathbf{V_1}$ will only be marginally shifted to negative values as a result of a weak interaction with **7** after the first reduction of $\mathbf{V_1}$. On the other hand, the first reduction potential of $\mathbf{V_2}$ will be considerably negatively shifted, thus maintaining the electrochemical gap between $\mathbf{V_1}$ and $\mathbf{V_2}$. This would exclude the formation of two co-existing radical cation viologens, $\mathbf{V_1}^{+\bullet}$ and $\mathbf{V_2}^{+\bullet}$. Additionally, their possible association is precluded by long and rigid bridge $\mathbf{B_2}$. Although, owing to the overlap of the second and the third reduction peaks, the observed electrochemical shift cannot be accurately measured, it is clear that the second reduction peak is slightly shifted towards more negative values and there is no unusual positive shift associated with dimerisation. Finally, the second reduction potential of $\mathbf{V_2}$ in **3**·PF_6 (−1.58 V) is substantially displaced towards more negative values compared with **4**·PF_6 (−1.48 V), which indicates that **7** populates $\mathbf{V_2}$ in the reduced state, **3**·PF_6.

Proposed co-conformational and conformational changes in **3** in solution are shown in Figure 3. It can be concluded that the population of the viologen sites by **7** changes over the course of four consecutive reduction steps. In the first oxidation state (**3**·4 PF_6), crown ether **7** predominantly populates $\mathbf{V_1}$. Predominant population of $\mathbf{V_2}$ takes place in **3**·3 PF_6, **3**·2 PF_6 (after double reduction) and in **3**·PF_6 (after triple reduction).

Comparing the two rotaxane systems it is noted that, unlike in **1**, the inversion of the site population (switching) happens in **3** after the first single-electron reduction. A likely explanation is that in **1**·3 PF_6 flexible bridge $\mathbf{B_1}$ folds back, which allows additional stabilisation of **7** at $\mathbf{V_1}$ by possible simultaneous interaction with both $\mathbf{V_1}$, and to a lesser extent, $\mathbf{V_2}$. On the contrary, in **3**·3 PF_6 rigid bridge $\mathbf{B_2}$ excludes the possibility of such additional stabilisation.

Conclusion

The observation of intramolecular shuttling processes in solution and at the surface is a challenging task for modern structural techniques because the changes in the spectral characteristics of switching molecular systems are subtle.

A ^{1}H NMR spectroscopy study of switchable **1**·4 PF_6 and **3**·4 PF_6 in solution demonstrates that the crown ether is located at the $\mathbf{V_1}$ recognition site in the parent state. The PRE technique can be used to determine the population of the recognition sites and the conformation of the first reduced states of **1**·3 PF_6 and **3**·3 PF_6. It can be demonstrated that in **1**·4 PF_6 the folding of the bridge interconnecting $\mathbf{V_1}$ and $\mathbf{V_2}$ results in additional stabilisation of the crown ether at $\mathbf{V_1}$. Consequently, the crown ether populates this site in the first reduced state, **1**·3 PF_6. The electrochemical behaviour of **1**·4 PF_6 further demonstrates that the crown ether populates $\mathbf{V_1}$ even in the second reduced state (**1**·2 PF_6).

In the case of **3**·4 PF_6, the possibility of bridge folding is precluded in all reduction states. Consequently, switching

(when the population of $\mathbf{V_2}$ is higher than $\mathbf{V_1}$) happens after the first reduction of **3**. However, even in this case the repositioning of the crown ether from $\mathbf{V_1}$ to $\mathbf{V_2}$ is not complete after the first reduction. This incomplete switching is possibly owing to low affinity of the crown ether for $\mathbf{V_2}$.

A comparison of the electrodynamics of switchable tripodal [2]rotaxanes **1**·4PF_6 and **3**·4PF_6 in solution strongly suggests that the design of the bridge between $\mathbf{V_1}$ and $\mathbf{V_2}$ in these [2]rotaxanes determines the degree of pre-organisation of the [2]rotaxane and its ability to switch. This implication is valuable for the development and design of new, more effective switchable molecular systems and is in good agreement with the most recent findings published by Stoddart and co-workers.[16]

Experimental Section

General methods: Reagents were purchased from Sigma-Aldrich. All reactions were conducted in a nitrogen atmosphere. Melting points were estimated by using a Gallenkamp melting point device and were not corrected. NMR spectra were recorded by using Varian Inova 300 and 500 spectrometers in the solvent indicated at 25 °C. Proton NMR spectra were recorded at 299.89 and 499.82 MHz and phosphorus NMR spectra at 121.39 MHz. Mass spectra were recorded by using a Micromass LCT mass spectrometer. Crystal data were collected by using a Bruker SMART APEX CCD area detector diffractometer. Paramagnetic suppression NMR spectroscopy was carried out as described elsewhere.[13c] Tripodal [2]rotaxane **1**·4PF_6 and axle **2**·4PF_6,[12] tripods **5**·2PF_6 and **8**·PF_6,[11] crown ether **7**,[30a] stopper bromide **13**,[10] and viologen **14**·2PF_6[30b,c] were prepared as described elsewhere.

Compound 6·2PF_6: Bromide **13** (0.076 g, 0.1 mmol) and 3,3′-dimethyl-4,4′-bipyridyl (0.009 g, 0.05 mmol) were added to a mixture of CH_3CN (2 mL) and CH_2Cl_2 (2 mL) and the mixture was left at room temperature for 6 d. The mixture was separated by column chromatography (silica gel; acetone/MeOH/nitromethane/saturated aqueous KPF_6 50:35:10:5 v/v), the retained fraction was evaporated under reduced pressure, the residue was extracted with CH_3Cl, the organic layer was washed with water and evaporated under reduced pressure to give **6** as a white solid (0.070 g, 70 %). M.p. 226 °C; ^{1}H NMR (300 MHz, CD_3CN, 25 °C): δ = 8.77 (s, 2H), 8.67 (d, J = 6.0 Hz, 2H), 7.74 (d, J = 6.0 Hz, 2H), 7.44 (d, J = 9.0 Hz, 4H), 7.30 (d, J = 9.0 Hz, 12H), 7.14–7.20 (m, 16H), 7.03 (d, J = 9.0 Hz, 4H), 6.80 (d, J = 9.0 Hz, 4H), 5.66 (s, 4H), 4.14–4.18 (m, 4H), 4.08–4.12 (m, 4H), 3.83–3.88 (m, 8H), 2.087 (s, 6H), 1.27 ppm (s, 54H); MS (ES): m/z (%): 865.5 (100) [**6**$^+$⁻stopper], 846.5 (45) [**6**·PF_6^{2+}]; elemental analysis calcd (%) for $C_{108}H_{126}F_{12}N_2O_6P_2$: C 70.57, H 6.91, N 1.52; found: C 70.80, H 6.83, N 1.74.

1,4-Bis(4-hydroxymethylphenyl)-2,5-dimethylbenzene: 1,4-Dibromo-2,5-dimethylbenzene (0.264 g, 1 mmol), 4-hydroxymethylboronic acid (0.320 g, 2.1 mmol), toluene (2 mL), ethanol (6 mL), potassium hydrogen phosphate (0.700 g, 5 mmol) and dichloro-1,1′-bis-(diphenylphosphinoferrocene)palladium dicholomethane (0.016 g, 0.02 mmol) were heated with stirring at 70 °C for 36 h. The mixture was extracted with EtOAc and purified by column chromatography (silica gel; EtOAc) to give the product as a white solid (0.24 g, 75 %). M.p. 167 °C; ^{1}H NMR (300 MHz, MeOH, 25 °C): δ = 7.40 (d, J = 8.0 Hz, 4H), 7.32 (d, J = 8.0 Hz, 4H), 7.10 (s, 2H), 4.67 (s, 4H), 2.23 ppm (s, 6H); elemental analysis calcd (%) for $C_{22}H_{22}O_2$: C 82.99, H 6.96; found: C 82.66, H 6.86. The product was crystallised from CH_3Cl/MeOH and monoclinic needles that were suitable for X-ray diffractometry analysis were obtained.

Compound 9: 1,4-Bis(4-hydroxymethylphenyl)-2,5-dimethylbenzene (0.064 g, 0.2 mmol) was suspended in THF (2 mL) and phosphorus tribromide (0.110 g, 0.4 mmol) was added. After stirring at room temperature for 3 h the mixture was diluted with diethyl ether, washed with aqueous sodium hydrogen carbonate, dried over $MgSO_4$ and evaporated under reduced pressure to give **9** as a white solid (0.088 g, 100 %). M.p. 172 °C; ^{1}H NMR (300 MHz, $CDCl_3$, 25 °C): δ = 7.45 (d, J = 8.0 Hz, 4H), 7.34 (d, J = 8.0 Hz, 4H), 7.13 (s, 2H), 4.57 (s, 4H), 2.27 ppm (s, 6H); elemental analysis calcd (%) for $C_{22}H_{20}Br_2$: C 59.49, H 4.54, Br 35.98; found: C 59.58, H 4.28, Br 35.87.

Compound 10·2PF_6: Monocation **8**·PF_6 (0.050 g, 0.04 mmol) and **9** (0.045 g, 0.1 mmol) were dissolved in benzonitrile (0.2 mL) and the mixture was kept at 36 °C for 2 d. The mixture was purified by column chromatography (silica gel; MeOH/nitromethane/saturated aqueous KPF_6 80:19:1 v/v) to give **10**·2PF_6 as a yellow solid (0.059 g, 83 %). Decomp 220–230 °C; ^{1}H NMR (300 MHz, CD_3OD, 25 °C): δ = 9.21 (d, J = 7.0 Hz, 2H), 9.18 (d, J = 7.0 Hz, 2H), 8.64 (d, J = 7.0 Hz, 2H), 8.57 (d, J = 7.0 Hz, 2H), 7.87–7.95 (m, 6H), 7.70–7.75 (m, 10H), 7.55–7.65 (m, 8H), 7.42–7.58 (m, 10H), 7.31 (d, J = 7.0 Hz, 2H), 7.10–7.14 (m, 2H), 5.93 (s, 2H), 4.58 (s, 2H), 4.00–4.18 (m, 12H), 2.24 (s, 6H), 1.35 ppm (t, J = 7.0 Hz, 18H); ^{31}P NMR: δ = 20.81 (s), −140 (septet, J = 711 Hz); MS (ES): m/z (%): 1475 (19) [**10**$^+$]; elemental analysis calcd (%) for $C_{87}H_{86}BrF_{12}N_2O_9P_5$: C 59.16, H 4.91, N 1.59; found: C 58.90, H 4.76, N 1.61.

Compound 12·3PF_6: Dication **10**·2PF_6 (0.058 g, 0.033 mmol) and 3,3′-dimethylbypiridyl (**11**, 0.016 g, 0.09 mmol) were dissolved in benzonitrile (0.16 mL) and the mixture was kept at room temperature for 6 d. Chromatography (silica gel; MeOH/nitromethane/saturated aqueous KPF_6 70:20:10 v/v) gave **12**·3PF_6 as a beige solid (0.055 g, 83 %). Decomp 230 °C; ^{1}H NMR (300 MHz, CD_3OD, 25 °C): δ = 9.18 (d, J = 6.2 Hz, 2H), 9.12 (d J = 6.2 Hz, 2H,), 8.92 (s, 1H), 8.76 (d, J = 6.2 Hz, 1H), 8.56–8.65 (m, 6H), 7.78–7.85 (m, 7H), 7.66–7.73 (m, 10H), 7.58–7.63 (m, 8H), 7.40–7.44 (m, 13H), 7.04 (s, 2H), 5.90 (s, 2H), 5.80 (s, 2H), 4–4.2 (m, 12H), 2.30 (s, 3H), 2.17 (s, 6H), 2.12 (s, 3H), 1.35 (t, J = 7.1 Hz, 18H); ^{31}P NMR: δ = 23.8 (s), −140 ppm (septet, J = 711 Hz); MS (ES): m/z (%): 1869 (30) [**12**·2PF6$^+$]; elemental analysis calcd (%) for $C_{99}H_{98}F_{18}N_4O_9P_6$: C 58.99, H 4.90, N 2.78; found: C 58.89, H 4.66, N 2.70.

[2]Rotaxane 3·4PF_6: Trication **12**·3PF_6 (0.053 g, 0.026 mmol), crown ether **7** (0.038 g, 0.071 mmol) and stopper **13** (0.038 g, 0.05 mmol) were dissolved in benzonitrile (0.15 mL) and kept at ambient temperatures for 10 d. Chromatography (silica gel; MeOH/nitromethane/saturated aqueous KPF_6 70:20:10 then MeOH/nitromethane/1 M aqueous NH_4PF_6 70:20:10 v/v) followed by extraction with nitromethane gave **3**·4PF_6 as a red solid (0.060 g, 69 %). M.p. 160 °C; ^{1}H NMR (500 MHz, CD_3CN, 25 °C): δ = 9.18 (d, J = 7.0 Hz, 2H), 8.98 (d, J = 7.0 Hz, 2H), 8.88 (s, 1H), 8.79 (s, 1H), 8.76 (d, J = 6.2 Hz, 1H), 8.69 (d, J = 6.2 Hz, 1H), 8.04 (d, J = 7.0 Hz, 2H), 7.92 (d, J = 7.0 Hz, 2H), 7.75–7.90 (m, 18H), 7.74 (d, J = 8.0 Hz, 6H), 7.50–7.64 (m, 10H), 7.40–7.46 (m, 4H), 7.30–7.34 (m, 6H), 7.16–7.22 (m, 10H), 7.03 (d, J = 9.0 Hz, 2H), 6.80 (d, J = 9.0 Hz, 2H) 6.16 (s, 8H), 5.99 (s, 2H), 5.80 (s, 2H), 5.67 (s, 2H), 4.15–4.20 (m, 4H), 4.08–4.15 (m, 12H), 3.82–3.90 (m, 4H), 3.55–3.70 (m, 24H), 3.45–3.50 (m, 8H), 2.25 (s, 6H), 2.22 (s, 3H), 2.20 (s, 3H), 1.29 (t, J = 7.1 Hz, 18H), 1.27 (s, 27H); ^{31}P NMR: δ = 23.70 (s), −140 ppm (septet, J = 712 Hz); MS (ES): m/z (%): 1543.5 (100) [**3**·2PF_6^{2+}]; elemental analysis calcd (%) for $C_{175}H_{195}F_{24}N_4O_{22}P_7$: C 62.20; H 5.82; N 1.66; found: C 62.26; H 5.54; N 1.51.

Axle 4·4PF_6: Trication **12**·3PF_6 (0.040 g , 0.02 mmol) and **13** (0.021 g, 0.028 mmol) were dissolved in benzonitrile (0.1 mL) and kept at room temperature for 10 d. Chromatography (silica gel; MeOH/nitromethane/saturated aqueous KPF_6 70:20:10; then MeOH/nitromethane/1 M aqueous NH_4PF_6 70:20:10 v/v) followed by extraction with nitromethane gave **4**·4PF_6 as a beige solid (40 mg, 70 %). Decomp 200–210 °C; ^{1}H NMR (300 MHz, CD_3COCD_3, 25 °C): δ = 9.60 (d, J = 7.1 Hz, 2H), 9.58 (d, J = 7.1 Hz, 2H), 9.42 (s, 1H), 9.32 (s, 1H), 9.27 (d, J = 7.1 Hz, 1H), 9.18 (d, J = 7.1 Hz, 1H), 8.96 (d, J = 7.1 Hz, 2H), 8.91 (d, J = 7.1 Hz, 2H), 8.20–8.24 (m, 2H), 8.04 (d, J = 9.0 Hz, 2H), 7.70–7.92 (m, 22H), 7. 63 (d, J = 9.0 Hz, 2H), 7.45–7.54 (m, 12H), 7.3 (d, J = 6.2 Hz, 6H), 7.10–7.14 (m, 12H), 6.82 (d, J = 9.0 Hz, 2H), 6.26 (s, 2H), 6.13 (s, 2H), 5.98 (s, 2H), 4.05–4.20 (m, 16H), 3.85–3.92 (m, 4H), 2.42 (s, 3H), 2.40 (s, 3H), 2.26 (s, 6H), 1.29 (t, J = 7.2 Hz, 18H), 1.28 (s, 27H); ^{31}P NMR: δ = 23.70 (s), −140 ppm (septet, J = 712 Hz); MS (ES): m/z (%): 1275.8 (100)

[**4**·2PF_6^{2+}]; elemental analysis calcd (%) for $C_{147}H_{155}F_{24}N_4O_{12}P_7$: C 62.11; H 5.50; N 1.97; found: C 61.96; H 5.50; N 1.81.

Cyclic voltammetry: All cyclic voltammograms were recorded in solution under the following conditions: The working electrode was an isolated platinum wire. The counter electrode was an isolated platinum foil. The reference electrode was a non-aqueous Ag/Ag^+ electrode filled with 10 mM $AgNO_3$ in the electrolyte solution. The electrolyte solution was tetraethylammonium hexafluorophosphate (0.05 mol dm^{-3}) in dry CH_3CN (distilled over calcium hydride). All solutions were degassed by three freeze–thaw cycles under vacuum prior to measurement. All cyclic voltammograms were recorded by using a Solartron SI 1287 potentiostat controlled by a LabView program running on a Macintosh Power PC at a scan rate of 10 mV s^{-1} unless otherwise stated.

Acknowledgement

This research was funded by Science Foundation Ireland and EU Marie Curie Host Development grants.

[1] a) P. W. K. Rothemund, *Nature* **2006**, *440*, 297–302; b) D. Philp, J. F. Stoddart, *Angew. Chem. Int. Ed. Engl* **1996**, *35*, 1154–1196; *Angew. Chem.* **1996**, *108*, 1242–1286; c) F. Mancin, E. Rampazzo, P. Tecilla, U. Tonellato, *Chem. Eur. J.* **2006**, *12*, 1844–1854; d) P. M. Mendes, S. Jacke, K. Critchley, J. Plaza, Y. Chen, K. Nikitin, R. E. Palmer, J. A. Preece, S. D. Evans, D. Fitzmaurice, *Langmuir* **2004**, *20*, 3766–3768.

[2] a) C. V. Cojocaru, F. Ratto, C. Harnagea, A. Pignolet, F. Rosei, *Microelectron. Eng.* **2005**, *80*, 448–456; b) D. Bishop, *Bell Lab. Technical Journal* **2005**, 23–28; c) W. Bows, *Investors Chronicle* **2002**, *139*, 30; d) J. E. Green, J. W. Choi, A. Boukai, Y. Bunimovich, E. Johnston-Halperin, E. DeIonno, Y. Luo, B. A. Sheriff, K. Xu, Y. S. Shin, H.-R. Tseng, J. F. Stoddart, J. R. Heath, *Nature* **2007**, *445*, 414–417; e) Y. Luo, C. P. Collier, J. O. Jeppesen, K. A. Nielsen, E. DeIonno, G. Ho, J. Perkins, H.-R. Tseng, T. Yamamoto, J. F. Stoddart, J. R. Heath, *ChemPhysChem* **2002**, *3*, 519–525.

[3] a) C. T. Lin, M. T. Kao, K. Kurabayashi, E. Meyhofer, *Small* **2006**, *2*, 281–287; b) D. K. Smith, *Chem. Commun.* **2006**, 34–44; c) P.M Mendes, A. H. Flood, J. F. Stoddart, *Appl. Phys. A: Mater. Sci. Process.* **2005**, *80*, 1197–1209; d) G. M. Whitesides, J. P. Mathias, C. T. Seto, *Science* **1991**, *254*, 1312–1319.

[4] a) J.-M. Lehn, *Supramolecular Chemistry, Concepts and Perspectives*, VCH, Weinheim, **1995**; b) R. J Forster, T. E. Keyes, J. G. Vos, *Interfacial Supramolecular Assemblies*, Wiley, Chichester, **2003**.

[5] a) R. F. Service, *Science* **1997**, *277*, 1036–1037; b) L, Cusack, S. N. Rao, D. Fitzmaurice, *Chem. Eur. J.* **1997**, *3*, 202–207.

[6] a) C. Niemeyer, *Angew. Chem.* **2001**, *113*, 4254–4287; *Angew. Chem. Int. Ed.* **2001**, *40*, 4128–4158; b) J. J. Davis, *Chem. Commun.* **2005**, 3509–3513; c) R. J. Alvarado, J. Mukherjee, E. J. Pacsial, D. Alexander, F. M. Raymo, *J. Phys. Chem. B* **2005**, *109*, 6164–6173.

[7] a) J. Berna, D. A. Leigh, M. Lubomska, S. M. Mendoza, E. M. Perez, P. Rudolf, G. Teobaldi, F. Zerbetto, *Nat. Mater.* **2005**, *4*, 704–710; b) A. Shipway, I. Willner, *Acc. Chem. Res.* **2001**, *34*, 421–432; c) F. Cecchet, P. Rudolf, S. Rapino, M. Margotti, F. Paolucci, J. Baggerman, A. M. Brouwer, E. R. Kay, J. K. Y. Wong , D. A. Leigh, *J. Phys. Chem. B* **2004**, *108*, 15192–15199; d) W. R. Browne, B. L. Feringa, *Nat. Nanotechnol.* **2006**, *1*, 25–35; e) E. R. Kay, D. A. Leigh, F. Zerbetto, *Angew. Chem.* **2007**, *119*, 72–196; *Angew. Chem. Int. Ed.* **2007**, *46*, 72–191.

[8] a) K. G. Thomas, P. V. Kamat, *Acc. Chem. Res.* **2003**, *36*, 888–898; b) U. Drechsler, B. Erdogan, V. M. Rotello, *Chem. Eur. J.* **2004**, *10*, 5570–5579; c) S. Mann, W. Shenton, M. Li, S. Connolly, D. Fitzmaurice, *Adv. Mater.* **2000**, *12*, 147–150; d) A. P. Alivisatos, *Science* **1996**, *271*, 933–937; e) A. Hagfeldt, M. Grätzel, *Chem. Rev.* **1995**, *95*, 49–68.

[9] a) E. Galoppini, W. Guo, P. Qu, G. J. Meyer, *J. Am. Chem. Soc.*, **2001**, *123*, 4342–4343; b) E. Galoppini, W. Guo, W. Zhang, P. G. Hoertz, P. Qu, G. J. Meyer *J. Am. Chem. Soc.*, **2002**, *124*, 7801–7811; c) L. Wei, K. Padmaja, W. J. Youngblood, A. B. Lysenko, J. S. Lindsey, D. F. Bocian, *J. Org. Chem.* **2004**, *69*, 1461–1469.

[10] K. Nikitin, B. Long, D. Fitzmaurice, *Chem. Commun.* **2003**, 282–283.

[11] B. Long, K. Nikitin, D. Fitzmaurice, *J. Am. Chem. Soc.* **2003**, *125*, 5152–5160.

[12] B. Long, K. Nikitin, D. Fitzmaurice, *J. Am. Chem. Soc.* **2003**, *125*, 15490–15498.

[13] a) S. Altobello, K. Nikitin, J. K. Stolarczyk, E. Lestini, D. Fitzmaurice, *Chem. Eur. J.* **2008**, *14*, 1107–1116 (preceding article); b) the term conformation is used herein to indicate any rotational conformation of the components of the [2]rotaxane and co-conformation is used to indicate the relative position of the crown ether in a [2]rotaxane. c) K. Nikitin, D. Fitzmaurice, *J. Am. Chem. Soc.* **2005**, *127*, 8067–8076.

[14] a) P. R. Ashton, R. Ballardini, V. Balzani, A. Credi, K. R. Dress, E. Ishow, C. J. Kleverlaan, O. Kocian, J. A. Preece, N. Spencer, J. F. Stoddart, M. Venturi, S. Wenger, *Chem. Eur. J.* **2000**, *6*, 3558–3574; b) V. Balzani, M. Clemente-León, A. Credi, B. Ferrer, M. Venturi, A. H. Flood, J. F. Stoddart, *Proc. Natl. Acad. Sci. USA* **2006**, *103*, 1178–1183; c) C. P. Collier, E. W. Wong, M. Belohradský, F. M. Raymo, J. F. Stoddart, P. J. Kuekes, R. S. Williams, J.R Heath, *Science* **1999**, *285*, 391–394; d) C. P. Collier, G. Mattersteig, E. W. Wong, Y. Luo, K. Beverly, J. Sampaio, F. M. Raymo, J. F. Stoddart, J. R. Heath, *Science* **2000**, *289*, 1172–1175; e) S. J. Loeb, J. Tiburcio, S. J. Vella, *Chem. Commun.* **2006**, 1598–1600; f) A. C. Benniston, A. Harriman, P. Li, J. P. Rostron, R. W. Harrington, W. Clegg, *Chem. Eur. J.* **2007**, *13*, 7838–7851.

[15] a) Y. H. Jang, W. A. Goddard, *J. Phys. Chem. B* **2006**, *110*, 7660–7665; b) T. Yamamoto, H.-R. Tseng, J. F. Stoddart, V. Balzani, A. Credi, F. Marchioni, M. Venturi, *Collect. Czech. Chem. Commun.* **2003**, *68*, 1488–1514.

[16] a) S. Nygaard, K. C.-F. Leung, I. Aprahamian, T. Ikeda, S. Saha, B. W. Laursen, S.-Y. Kim, S. W. Hansen, P. C. Stein, A. H. Flood, J. F. Stoddart, J. O. Jeppesen, *J. Am. Chem. Soc.* **2007**, *129*, 960–970; b) J. W. Choi, A. H. Flood, D. W. Steuerman, S. Nygaard, A. B. Braunschweig, N. N. P. Moonen, B. W. Laursen, Y. Luo, E. DeIonno, A. J. Peters, J. O. Jeppesen, K. Xu, J. F. Stoddart, J. R. Heath, *Chem. Eur. J.* **2006**, *12*, 261–279.

[17] M. Asakawa, P. R. Ashton, R. Ballardini, V. Balzani, M. Bělohradský, M. T. Gandolfi, O. Kocian, L. Prodi, F. M. Raymo, J. F. Stoddart, M. Venturi, *J. Am. Chem. Soc.* **1997**, *119*, 302–310.

[18] F. M. Raymo, K. N. Houk, J. F. Stoddart, *J. Am. Chem. Soc.*; **1998**, *120*, 9318–9322.

[19] a) M. C. T. Fyfe, J. F. Stoddart, *Acc. Chem. Res.* **1997**, *30*, 393–401; b) P. L. Anelli, P. R. Ashton, R. Ballardini, V. Balzani, M. Delgado, M. T. Gandolfi, T. T. Goodnow, A. E. Kaifer, D. Philp, M. Pietraszkiewicz, L. Prodi, M. V. Reddington, A. M. Z. Slawin, N. Spencer, J. F. Stoddart, C. Vincent, D. J. Williams, *J. Am. Chem. Soc.* **1992**, *114*, 193–218.

[20] P. R. Ashton, R. Ballardini, V. Balzani, M. Belohradsky, M. T. Gandolfi, D. Philp, L. Prodi, F. M. Raymo, M. V. Reddington, N. Spencer, J. F. Stoddart, M. Venturi, D. J. Williams, *J. Am. Chem. Soc.* **1996**, *118*, 4931–4951.

[21] F. Huang, L. N. Zakharov, A. L. Rheingold, M. Ashraf-Khorassani, H. W. Gibson, *J. Org. Chem.* **2005**, *70*, 809–813.

[22] a) C. A. Hunter, *J. Am. Chem. Soc.* **1992**, *114*, 5303–5311; b) A. C. Benniston, A. Harriman, V. M. Lynch, *J. Am. Chem. Soc.* **1995**, *117*, 5275–5291.

[23] a) P. R. Ashton, R. Ballardini, V. Balzani, I. Baxter, A. Credi, M. C. T. Fyfe, M. T. Gandolfi, M. Gómez-López, M.-V. Martínez-Díaz, A. Piersanti, N. Spencer, J. F. Stoddart, M. Venturi, A. J. P. White, D. J. Williams, *J. Am. Chem. Soc.* **1998**, *120*, 11932–11942; b) J. F. Stoddart, S. A. Vignon, *Collect. Czech. Chem. Commun.* **2005**, 70, 1493–1576.

[24] The signal in the NOE spectrum that corresponds to protons H_{18} ($\delta = 6.0$) overlaps with the intense excitation peak of H_{13} ($\delta = 6.2$) in this case.

[25] It is noted that although in some cases the radical cations formed when a viologen undergoes a single-electron reduction may dimerise in solution, it has been shown that relatively bulky [2]rotaxanes are present as monomers in solution, see reference [13c] and J. A. Alden, J. A. Cooper, F. Hutchinson, F. Prieto, R. G. Compton, *J. Electroanal. Chem.* **1997**, *432*, 63–70.
[26] We assume that shuttling is fast on the NMR spectroscopy timescale and that bridge **B** represents a sufficiently high barrier and is not occupied itself.; see also: D. A. Leigh, A. Troisi, F. Zerbetto, *Angew. Chem.* **2000**, *112*, 358–361; *Angew. Chem. Int. Ed.* **2000**, *39*, 350–353.
[27] M. N. Chatterjee, E. R. Kay, D. A Leigh, *J. Am. Chem. Soc.* **2006**, *128*, 4058–4073.
[28] a) J. A. Alden, J. A. Cooper, F. Hutchinson, F. Prieto, R. G. Compton, *J. Electroanal. Chem.* **1997**, *432*, 63–70; b) L. Pospíšil, J. Fiedler, M. Hromadová, M. Gál, M. Valášek, J. Pecka, J. Michl, *J. Electrochem. Soc.* **2006**, *153*, E179–E183; c) X. Tang, T. W. Schneider, J. W. Walker, D. A. Buttry, *Langmuir* **1996**, 12, 5921–5933.
[29] The relatively low reduction potential of $\mathbf{V_2}$ in **6**·2PF6 (−1.55 V) is possibly associated with structural folding and encapsulation of the viologen moiety; a process that was demonstrated earlier in: F. Marchioni, M. Venturi, P. Ceroni, V. Balzani, M. Belohradsky, A. M. Elizarov, H.-R. Tseng, J. F. Stoddart, *Chem. Eur. J.* **2004**, *10*, 6361–6368.
[30] a) R. C. Helgeson, T. L. Tarnowski, J. M. Timko, D. J. Cram, *J. Am. Chem. Soc.* **1977**, *99*, 6411–6418; b) C. Stoehr, M. Wagner, *J. Prakt. Chem.* **1893**, *48*, 1; c) E. Lestini, K. Nikitin, H. Müller-Bunz, D. Fitzmaurice, *Chem. Eur. J.* **2008**, *14*, 1095–1106.

Received: September 3, 2007
Published online: November 28, 2007

